THE ASTROPHYSICAL JOURNAL, 469:311–319, 1996 September 20

A NEW MECHANISM FOR GAMMA-RAY BURSTS IN SN TYPE I EXPLOSIONS. I. WEAK MAGNETIC FIELD

V. S. BEREZINSKY
INFN, Laboratori Nazionali del Gran Sasso, Statale 17 bis 67010-Assergi (L'Aquila), Italy
P. BLASI
INFN, Laboratori Nazionali del Gran Sasso, and Universitá degli Studi di L'Aquila, via Vetoio, 67100-Coppito (L'Aquila), Italy
AND
B. I. HNATYK
Institute for Applied Problems in Mechanics and Mathematics, NASU, Naukova str. 3b, Lviv-53, 290053, Ukraine
Received 1995 November 8; accepted 1996 March 29

ABSTRACT

We propose a new mechanism for high-energy gamma-ray bursts in supernova type I (SN I) explosions. From their observational features, they are a new type of bursts, different from others observed. A presupernova is assumed to be a binary system made up of a red giant and a white dwarf with a wind accretion. The accretion flow is terminated by an accretion shock in the vicinity of the white dwarf at a distance of the order of the accretion radius. The gas inside the accretion radius constitutes the main fraction of the target for gamma-ray production.

The supernova explosion and the shock propagation in the white dwarf result in the hydrodynamical acceleration of the outer layers of the star. It proceeds in two stages: the first stage is caused by the shock propagating in the outer layers of the star, and the second stage is connected with the adiabatic expansion of the ejected shell into low-density medium around the white dwarf. The spectrum of accelerated particles is steep, and the maximum energy does not exceed 1000 GeV.

The gamma-ray burst is produced by the interaction of the accelerated particles with the gas in the binary system. Most of the photons have energies about 100 MeV. The total number of emitted photons is between 10^{46} and 10^{47}. The typical duration of the burst is $\sim$1–3 s for $\sim$100 MeV photons and 10^{-3} s for $\sim$1 GeV photons. Thus, the bursts can be detected at distances less than 1 Mpc, with frequency less or equal to that of SN I.

The gamma-ray burst might have one or two precursors. The first one is produced during the shock breakout, when the shock approaches the star surface and crosses it. This burst is produced by the heated gas behind the shock; the radiation is blueshifted because of the relativistic motion of the shell. The second burst might be produced under the appropriate choice of the parameters at the stage of the adiabatic expansion of the shell of the accelerated matter, when the shell becomes transparent for radiation.

Our calculations are valid in the case of a weak magnetic field. The case of strong magnetic field will be considered in Paper II (in preparation).

Subject headings: acceleration of particles — accretion, accretion disks — binaries: close — gamma rays: bursts — shock waves — supernovae: general

1. INTRODUCTION

It is possible that there are several different types of sources of observed gamma-ray bursts (GRB). If GRB have a cosmological origin, the repeaters are sources of one type. GRB with smooth and complex time profiles can be produced by two different types of sources. Probably burst radiation is a typical phenomenon for many types of sources.

Our aim is not to explain observed GRB but to search for reliable production mechanisms that might be discovered in the future. In this sense, our work is similar to that of Berezinsky & Prilutsky (1985), in which the mechanism of GRB caused by $\nu\bar{\nu}$ annihilation at the collapse of a compact object was suggested. At that time, this mechanism could not explain the observed GRB, but it was used later in connection with the study of the cosmological origin of GRB.

We propose a mechanism for GRB in SN I explosions. More specifically, we study SN Ia explosions, which, as is widely accepted, occur in a binary system composed of a carbon-oxygen white dwarf with nearly Chandrasekhar mass and a late-type secondary companion star (Wheeler & Harkness 1990; Khokhlov, Müller, & Höflich 1993).

The explosion is caused by the thermonuclear reactions caused by disk accretion (Nomoto 1982) or wind accretion (Munari & Renzini 1992; Kenyon et al. 1993) of the gas onto the white dwarf. The shock wave propagation through the outermost layer of the white dwarf accelerates a small part of it to relativistic and ultrarelativistic velocities, as was first suggested by Colgate & Johnson (1960). This acceleration is connected with the increase of the shock velocity when the shock propagates in a medium with decreasing density.

For a long time, the Colgate mechanism (for a review, see Colgate 1984) was one of the challengers for acceleration of the observed cosmic rays. Now there are convincing arguments, based on adiabatic energy losses and on the estimates of the rate of accelerated particles, that this is not the case (e.g., Woosley, Taam, & Weaver 1986).

It is most probably true that the Colgate mechanism cannot provide all of the observed pool of cosmic rays, but it is also true that this mechanism does work under appropriate physical conditions. In particular, it works in the case of shock propagation through the surface of a white dwarf. The interaction of accelerated particles with ambient gas results in the production of gamma radiation through p-p collisions, with the consequent π^0 production and decay.

In this paper, we investigate a gamma-ray burst produced by the interaction of accelerated particles with the accreting gas in the regime of wind accretion. In § 2, the space distribution of the gas in an accretion flow is considered. The propagation of the shock in the envelope of the white dwarf is studied in § 3. In § 4, we consider the additional acceleration of particles caused by the expansion of the shell in a low-density medium, and we calculate the resulting energy spectrum. The main gamma-ray burst, produced as a result of the interaction of accelerated particles with the accretion flow, is described in § 5. Discussion and conclusions are presented in § 6.

2. GAS DISTRIBUTION IN A PRESUPERNOVA BINARY SYSTEM

We shall concentrate mostly on SN Type Ia for which explosion occurs in the white dwarf. As a model for a presupernova, we shall consider a binary system consisting of a carbon-oxygen white dwarf and a red giant. The accretion to the white dwarf results in an explosion that occurs when the accreting gas accumulates on the carbon-oxygen interior of the compact companion and triggers the detonation with consequent mass ejection.

We shall consider the wind regime of accretion when the white dwarf accretes the gas from the companion's stellar wind (Kenyon et al. 1993; Munari & Renzini 1992). In this regime of accretion, an explosion is possible for a carbon-oxygen white dwarf with initial mass 0.5–1.3 $M_\odot$ and for an accretion rate of helium gas $\dot{M}_a \leq 4 \times 10^{-8}\ M_\odot\ \mathrm{yr}^{-1}$ (Fujimoto & Taam 1982).

Observationally, such systems correspond to the symbiotic stars. The observed orbital periods for these stars (1–10 yr) imply a separation of the binary components $d \simeq (2\text{–}9) \times 10^{13}$ cm. The secondary component generally does not fill its Roche lobe, and the mass loss is provided by the stellar wind at the rate of $\dot{M}_W \sim 10^{-7}\ M_\odot\ \mathrm{yr}^{-1}$ (Kenyon et al. 1993).

As a first approximation, the accretion from the stellar wind can be described by the classical theory of Hoyle & Littleton (1939). The parameters of this theory are the mass of the accreting star M_S, the density of the gas in the wind ρ_W, and its velocity with respect to the star u_W. The theory operates with the accretion radius R_{acc} and the accretion rate $\dot{M}_{\mathrm{HL}}$ given by

$$R_{\mathrm{acc}} = \frac{2GM_S}{u_W^2(d)} \tag{1}$$

and

$$\dot{M}_{\mathrm{HL}} = \pi R_{\mathrm{acc}}^2 \rho_W(d) u_W(d)\ , \tag{2}$$

where G is the gravitational constant and d is the separation of the stars. We shall assume a supersonic flow of the gas at a large distance from the star, $r \sim d$.

Recent numerical calculations for two-dimensional axisymmetric wind accretion were performed by Matsuda, Inoue, & Sawada (1987), Fryxell & Taam (1988), Taam & Fryxell (1988, 1989), and Taam, Fu, & Fryxell (1991). The hydrodynamical picture of the gas flow includes the shock, the region of stagnation $u_{\mathrm{acc}} \simeq 0$, a considerable density increase in the wake, and some other features. The flow critically depends on the accretion rate $\dot{M}_a$. For small accretion rates, $\dot{M}_a \ll \dot{M}_{\mathrm{Edd}}$, the flow is steady. For large $\dot{M}_a$, the flow probably exhibits a time variation. The details, essential for our calculations, are as follows. The shock is produced at a distance $R_{\mathrm{sh}} = \xi R_{\mathrm{acc}}$, with $\xi < 1$ and, typically, $\xi = 0.1$–0.2. The accretion rate is $\dot{M}_a = \eta \dot{M}_{\mathrm{HL}}$, where η can reach the large fraction $\eta \sim 0.6$.

Inspired by these results, we adopt the following simplified picture for the binary system and for the gas flow in it (Fig. 1). The compact star (white dwarf) and the secondary component (red giant) are separated by distance d. The red giant does not fill its Roche lobe, and its mass loss is caused by a stellar wind with supersonic velocity u_W. For our calculations, it is enough to assume a spherically symmetric shock with radius

$$R_{\mathrm{sh}} = \xi R_{\mathrm{acc}}\ . \tag{3}$$

Outside the shock, the density distribution is

$$\rho_W(r_{\mathrm{RG}}) = \frac{\dot{M}_W}{4\pi u_W r_{\mathrm{RG}}^2}\ , \tag{4}$$

where r_{RG} is the distance from the red giant. Inside the shock, we assume

$$\rho_a(r) = \rho_a(R_{\mathrm{sh}})(r/R_{\mathrm{sh}})^{-3/2}\ , \tag{5}$$

according to the calculations of Taam et al. (1991). Equation (5) corresponds to the quasi-spherical accretion inside the shock, with infall velocity proportional to the free-fall velocity

$$u_a(r) = \zeta u_{\mathrm{ff}}(r)\ , \tag{6}$$

where $u_{\mathrm{ff}} = (2GM_S/r)^{1/2}$ and $\zeta = \eta/(16\xi^{3/2})$. In our calculations, we use $\eta = 0.5$, $\xi = 0.2$, and, thus, $\zeta = 0.35$.

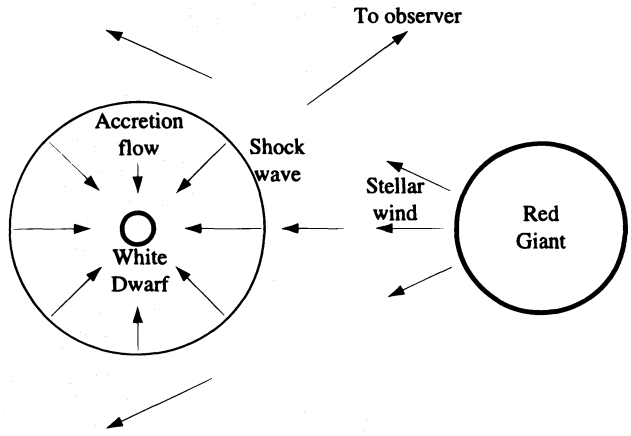

FIG. 1.—Schematic model of a presupernova Type Ia binary system. The secondary companion (red giant) loses matter via stellar wind, and the white dwarf accretes it in the regime of wind accretion.

TABLE 1

NUMERICAL VALUES OF WHITE DWARF AND WIND ACCRETION FLOW PARAMETERS

Parameters	Compact White Dwarf	Extended White Dwarf
R_S (cm)	1.0×10^8	1.0×10^9
$M_S/M_\odot$	1.4	1.0
ρ_0 (g cm^{-3})	1.0×10^{12}	4.0×10^9
d (cm)	3.0×10^{13}	3.0×10^{13}
R_{sh} (cm)	8.3×10^{12}	5.9×10^{12}
$\dot{M}_a$ ($M_\odot$ yr^{-1})	2.4×10^{-8}	1.2×10^{-8}
$\dot{M}_W$ ($M_\odot$ yr^{-1})	1.0×10^{-7}	1.0×10^{-7}
u_W (cm s^{-1})	3.0×10^6	3.0×10^6
$x(r \le R_{sh})$ (g cm^{-2})	3.4	0.67

We assume a density jump on the surface of the shock, as in the strong shock

$$\rho_a(R_{sh}) = 4\rho_W(d) . \tag{7}$$

The numerical values that we use in the calculations are presented in Table 1. The notation used in Table 1 is as follows: R_S and M_S are the radius and the mass of the white dwarf, respectively; ρ_0 is given by equation (8); d is the separation of the stars in the binary; R_{sh} is the radius of the accretion shock; $\dot{M}_a$ is the rate of accretion onto the white dwarf; $\dot{M}_W$ is the rate of mass loss by the secondary component of the binary; u_W is the wind velocity; and $x_{sh} = \int_{R_S}^{R_{sh}} \rho(r)dr$ is the column density of accreting gas inside the shock.

3. THE RELATIVISTIC SHOCK IN SN I AND THE PRECURSOR GAMMA-RAY BURST

Explosive nuclear burning in the white dwarf produces an outward-moving shock. In this section, we shall study the propagation of the shock in the outer layers of the white dwarf and beyond.

The process of thermonuclear burning propagates in the compact star, either in the form of a supersonic detonation wave with velocity $(1.1–1.4) \times 10^9$ cm s^{-1}, or in the regime of a subsonic deflagration wave (Khokhlov et al. 1993). The latter can be converted into a detonation wave in the outer layers of the star, where the pressure gradient is high. We shall limit our consideration to the propagation of the shock in the periphery of the star, where the typical shock velocity is $u_{sh} \ge 10^9$ cm s^{-1}. The density of the gas in the considered outer layer is characterized by a large gradient. In our estimates, we use the polytropic model with $n = 3$, for which the density is

$$\rho(r) = \rho_0\left(1 - \frac{r}{R_S}\right)^3 , \tag{8}$$

where ρ_0 is a constant and R_S is the radius of the star. The propagation of the shock in the outermost layers of a white dwarf with large density gradient results in the growth of the shock velocity up to the relativistic regime (Colgate & Johnson 1960). The velocity of the strong adiabatic shock wave propagation in the medium with large density gradient $-d\ln\rho/d\ln r \gg 1$, in both the nonrelativistic and relativistic regimes, may be approximated by the expression given by Gnatyk (1985):

$$\Gamma_{sh}\beta_{sh} = \text{const} \times \rho^{-a} , \tag{9}$$

where $\beta_{sh} = u_{sh}/c$ is the dimensionless velocity of the shock, c is the velocity of light, and $\Gamma_{sh} = (1 - \beta_{sh}^2)^{-1/2}$ is the Lorentz factor of the shock. The parameter a in this approximation is $a \approx 0.2$ for both nonrelativistic and relativistic shock waves. Analytical solutions for the nonrelativistic shock wave propagation in exponential and polytropic density distributions give the values $0.17 \le a \le 0.23$, for adiabatic index $4/3 \le \gamma_{ad} \le 5/3$ and for polytropic index $1.5 \le n \le 3.25$. For the ultrarelativistic shock that Johnson & McKee (1971) obtained analytically, the value is $a = 0.232$. In our calculation, we shall consider two extreme possibilities: $a = 0.2$ and $a = 0.232$.

Let us now calculate the maximum value of $\Gamma_{sh}\beta_{sh}$ for the shock in the star. Following Colgate (1984), we use, instead of r, another variable F, which is the fraction of the star mass beyond radius r. Using equation (8), one obtains

$$F = \rho^{4/3}\frac{\pi R_S^3}{M_S\rho_0^{1/3}} . \tag{10}$$

Introducing the initial condition $\Gamma_{sh}\beta_{sh} = (\Gamma_{sh}\beta_{sh})_i$ at $F = F_i$, we obtain for the shock velocity in the shell

$$\Gamma_{sh}\beta_{sh} = (\Gamma_{sh}\beta_{sh})_i\left(\frac{F}{F_i}\right)^{-3a/4} . \tag{11}$$

The numerical calculations (Khokhlov et al. 1993, and references therein) show that the shock starts to be accelerated effectively at the depth $F_i \sim 0.05$. This is caused by the large density gradient in the outer layers of the white dwarf. Hereafter we use $F_i = 0.05$ as the initial value. According to the above mentioned numerical calculations, the velocity of the shock at $F = F_i$ is

$$(\beta_{sh})_i = 5 \times 10^{-2}k_s , \tag{12}$$

with k_s between 0.7 and 1.0. We shall use for our calculations $k_s = 1.0$.

The maximum value of $\Gamma_{sh}\beta_{sh}$ corresponds to the smallest value of F at which the shock still exists in the outer, highly rarefied layer. The shock breaks out at the radius r_{max}, where the dissipation of energy caused by the escape of photons or other particles becomes essential. In the case of radiation-dominated nonrelativistic SN II shock, this condition can be expressed as an equality between the optical thickness of photons and the front thickness (Imshennik & Nadyozin 1989; Ensman & Burrows 1992). In the case of relativistic SN shock, the condition for the shock breakout can be understood as the equality of the path length of the nucleus in the shock transition zone and the residual thickness of this layer (Colgate 1974, 1984). Using equations (8) and (10), one obtains

$$F_{min} = \frac{4\pi R_S^2 x_{int}}{M_S} , \tag{13}$$

where x_{int} is the interaction path length of nuclei in g cm^{-2}. Substituting this value of F_{min} into equation (11), one obtains

$$(\Gamma_{sh}\beta_{sh})_{max} = (\Gamma_{sh}\beta_{sh})_i\left(\frac{4\pi R_S^2 x_{int}}{M_S F_i}\right)^{-3a/4} . \tag{14}$$

The value of x_{int} depends on the physical conditions in the shock transition zone. For the relativistic shock waves considered here, the main source of shock dissipation is ion-lepton dynamical friction (Colgate 1974; Weaver 1976). In the compact white dwarf case, the temperature at the shock front nearby the surface is of the order of

$(3–4) \times 10^8$ K (see below), and the number density of electron-positron pairs reaches 10^{23}–10^{24} cm^{-3}. The main energy losses of ions in this case are caused by elastic nucleus-electron scattering and bremsstrahlung radiation. The path length of ions is 1–3 g cm^{-2}. In the extended white dwarf case, the temperature at the surface is lower, and the energy losses are dominated by pion production. However, deeper in the star at $x \sim 10$ g cm^{-2}, the temperature is again high enough for e^+e^- production, and the effective path length can be taken as $x_{\rm int} \sim 10$ g cm^{-2}. Fortunately, according to equation (14), $(\Gamma_{\rm sh}\beta_{\rm sh})_{\rm max}$ weakly depends on $x_{\rm int}$, typically as $x_{\rm int}^{-0.15}$. In the calculations below, we use $x_{\rm int} = 3$ g cm^{-2}. Equations (11) and (14) describe the propagation of the shock through the outer layers of the star; in other words, equation (11) gives the value of $\Gamma\beta$ for the shock at the various positions F, and equation (14) gives the maximum value of $\Gamma\beta$ at the moment when the shock reaches the surface of the star.

Now we shall proceed with the calculations of the velocity of the gas and its thermodynamical characteristics behind the shock. After the shock crosses a layer of the gas, this layer acquires a radial velocity that is somewhat smaller than the shock velocity. The gas behind the shock is also heated to a high temperature. This is the first stage of hydrodynamical acceleration.

Let us give the typical values of $(\Gamma_{\rm sh}\beta_{\rm sh})_{\rm max}$ in our models. For the compact white dwarf model, with $M_S = 1.4\ M_\odot$, $R_S = 1 \times 10^8$ cm, and $\rho_0 = 1 \times 10^{12}$ g cm^{-3} (Table 2), $F_{\rm min}$ from equation (13) is 4.5×10^{-17}; hence, $(\Gamma_{\rm sh}\beta_{\rm sh})_{\rm max} = 9.0$ and 20 for $a = 0.2$ and $a = 0.232$, respectively. For the extended white dwarf model, with $M_S = 1.0\ M_\odot$, $R_S = 1 \times 10^9$ cm, and $\rho_0 = 4 \times 10^9$ g cm^{-3} (Table 1), we obtain $F_{\rm min} = 6.3 \times 10^{-15}$ and $(\Gamma_{\rm sh}\beta_{\rm sh})_{\rm max} = 4.3$ and 8.8 for $a = 0.2$ and $a = 0.232$, respectively. Note that these values are considerably smaller than those in the calculations made by Colgate (1984).

Heating and acceleration of the gas behind the strong adiabatic radiation-dominated ($\gamma_{\rm ad} = 4/3$) shock wave, which propagates in nonrelativistic cold gas, can be described in terms of the conditions on the shock front, as given by Blandford & McKee (1976):

$$\epsilon_2 = \Gamma_2(4\Gamma_2 + 3)\rho_1 c^2 , \tag{15}$$

$$\rho_2 = (4\Gamma_2 + 3)\rho_1, \tag{16}$$

$$\Gamma_{\rm sh}^2 = (4\Gamma_2 - 1)^2(\Gamma_2 + 1)/(8\Gamma_2 + 10) , \tag{17}$$

where indices 1 and 2 refer to the parameters in front of and behind the shock, respectively, $\Gamma_2 = (1 - \beta_2^2)^{-1/2}$ is the Lorentz factor of the fluid behind the shock, ρ is the density of the gas, and ϵ is the energy density.

TABLE 2

VALUES OF THE SHOCK AND GAS PARAMETERS AT THE MOMENT OF SHOCK WAVE BREAKOUT

	COMPACT WHITE DWARF		EXTENDED WHITE DWARF	
PARAMETERS	$a = 0.2$	$a = 0.232$	$a = 0.2$	$a = 0.232$
$F_{\rm min}$	4.5×10^{-17}	4.5×10^{-17}	6.3×10^{-15}	6.3×10^{-15}
$(\beta_{\rm sh}\Gamma_{\rm sh})_{\rm max}$ ...	9.0	21	4.3	8.8
$(\Gamma_2)_{\rm max}$	6.7	16	3.4	6.6
$T_2^{\rm sur}$ (K)	4.8×10^8	7.4×10^8	1.6×10^8	2.2×10^8
$\bar{E}_\gamma^{\rm obs}$ (keV) ...	280	1020	48	125

The equation of state of the gas behind the shock is given by

$$p_2 = \tfrac{1}{3}(\epsilon_2 - \rho_2 c^2) . \tag{18}$$

From equation (18), it is easy to obtain the following formula for the pressure:

$$p_2 = \tfrac{1}{3}(4\Gamma_2 + 3)(\Gamma_2 - 1)\rho_1 c^2 . \tag{19}$$

In our case, the main contribution to the pressure is provided by the radiation,

$$p_2 = \tfrac{1}{3}a_K T_2^4 \tag{20}$$

for $kT_2 \ll m_e c^2$, and by the radiation and the electron-positron pairs,

$$p_2 = \tfrac{1}{3}a_K T_2^4(1 + \tfrac{7}{4}) \tag{21}$$

for $kT_2 \gg m_e c^2$, where a_K is a constant of the energy density of radiation.

Hence, one obtains for $kT_2 \gg m_e c^2$ and $kT_2 \ll m_e c^2$, respectively,

$$T_2 = \left[\frac{4}{11a_K}(4\Gamma_2 + 3)(\Gamma_2 - 1)\rho_1 c^2\right]^{1/4} \tag{22}$$

and

$$T_2 = \left[(4\Gamma_2 + 3)(\Gamma_2 - 1)\frac{\rho_1 c^2}{a_K}\right]^{1/4} . \tag{23}$$

A comment to equation (17) is in order. This equation gives the connection between the Lorentz factor of the shock $\Gamma_{\rm sh}$ and the Lorentz factor Γ_2 of the fluid behind the shock. Therefore, from the known shock velocity at each F, given by equation (11), one can reconstruct, using equation (17), the distribution of the Lorentz factor of the gas over the outer layers at the moment when the shock reached the surface of the star. The maximum value of Γ_2 corresponds to the maximum value of $\Gamma_{\rm sh}$, given by equation (14). Numerically, for the compact white dwarf model, we obtain $(\Gamma_2)_{\rm max} = 6.7$ and 15 for $a = 0.2$ and $a = 0.232$, respectively. For the extended white dwarf model, we obtain $(\Gamma_2)_{\rm max} = 3.4$ and 6.6 for $a = 0.2$ and $a = 0.232$, respectively. According to equation (22), the large value of $(\Gamma_2)_{\rm max}$ results in the high temperature $T_2^{\rm sur}$ at the moment when the shock reaches the surface.

Let us now discuss the temperature of the gas behind the shock front and the precursor gamma-ray burst connected with it. When the shock reaches the surface of the star, the temperature $T_2^{\rm sur}$ behind it is given by equation (22), with $\Gamma_2 = (\Gamma_2)_{\rm max}$. The corresponding values for the compact model are $4.9 \times 10^8(7.4 \times 10^8)$ K for $a = 0.2(0.232)$, and the values for the extended model are $1.6 \times 10^8(2.2 \times 10^8)$ K for $a = 0.2(0.232)$.

The burst of radiation emerges from the star during the shock breakout, when radiation energy trapped in the shock escapes through the translucent external layer of the star. The shock breakout phenomenon was studied in detail for the case of SN II by Grassberg, Imshennik, & Nadyozhin (1971), Imshennik & Nadyozhin (1988, 1989), Blinnikov & Nadyozhin (1991), and Ensman & Burrows (1992). The picture can be described as follows. At the time the shock approaches the surface it becomes thick. When the precursor of the shock reaches the surface, the front is spread over the distance with the optical thickness $\tau \sim 100$, according to the calculations of Ensman & Burrows (1992). This moment

can be taken as one when the shock breakout starts and the radiation emerges from the star. Following this picture qualitatively, it is easy to evaluate the total energy of the burst in the relativistic case that we are examining. In the rest system of the shock, this is given by the product of $4\pi R_s^2 \sigma (T_2^{\rm sur})^4$ and the duration of the burst. The latter can be estimated as the time ($\delta t_{\rm rest} \sim l_\gamma/c$) of the photon escape from the thickness (l_γ) of the shock front. For the compact dwarf, scattering of the photons is caused mainly by e^+e^- pairs (for the extended dwarf their contribution is rather small). Then l_γ for optical thickness $\tau \sim 100$ is given by $l_\gamma \sim \tau(\sigma_{\rm T} n_{e^+e^-})^{-1} \sim 2.5 \times 10^2 (2.5)$ cm for $a = 0.2(0.232)$. Taking into account the blueshift of the emitted photons, the fluency F_γ is found to be

$$F_\gamma = (\Gamma_2)_{\rm max} 4\pi R_s^2 \sigma (T_2^{\rm sur})^4 l_\gamma/(4\pi r^2 c) ,$$

where r is the distance to the source. Numerically, this fluency is $F_\gamma \sim 2 \times 10^{-6}$ ergs cm^{-2} for $r = 10$ kpc and the compact dwarf model with $a = 0.2$. For the extended white dwarf model, this flux is $\sim 10^{-2}$ times larger. The typical energy of the photons in the burst is $E_\gamma^{\rm obs} \sim (\Gamma_2)_{\rm max} k T_2^{\rm sur} \sim$ 300(1000) keV for the case of the compact white dwarf with $a = 0.2(0.232)$. The values of the temperature $T_2^{\rm sur}$ and the mean energy of the photons from the precursor burst are tabulated in Table 2. The duration of the burst $\delta t_{\rm obs}$, as observed by a distant observer, is very short. The duration is determined by the time delay of the photons arriving from the different points of the star surface. The beaming effect makes the duration shorter in the relativistic case (see, e.g., Rees 1966). Since the emitting angle is $\theta_e \sim 1/\Gamma$ in the laboratory frame, the time delay of the photons from the $\theta = 0$ and $\theta = \theta_e$ directions is

$$(\delta t)_{\rm obs} \sim \frac{R_s}{c} \frac{1}{2\Gamma_2^2} , \qquad (24)$$

which numerically is $4 \times 10^{-5} (7 \times 10^{-6})$ s for $a = 0.2(0.232)$.

The accurate calculations are needed for the detailed description. However, the gamma-ray precursor due to the shock breakout seems to be detectable by such instruments as BATSE.

4. HYDRODYNAMICAL ACCELERATION

Hydrodynamical acceleration proceeds in two stages. During the first stage, described in § 3, the shock propagating through the gas with the falling density increases its velocity according to equation (11), until the fraction of the shell ahead of it reaches $F_{\rm min}$, given by equation (13). Starting from this moment the shock is decaying. It leaves behind the heated shell, moving outward with velocity β_2, as well as Lorentz factor Γ_2, given by equation (17). The shell now expands in the low-density gas. The thermal energy of the shell, as well as the work of the pressure of the inner layers, are converted into kinetic energy of the shell. This is the second, adiabatic stage of acceleration.

When the shock reaches the surface of the star, the shell has a wide-velocity distribution from nonrelativistic values in the inner parts of the shell to ultrarelativistic ones in the narrow outer part of the shell. During the adiabatic stage, the nonrelativistic velocities of gas elements increases as $u_f \simeq 2k_N u_2$, where u_f and u_2 are the final and initial velocities, respectively, and we take $k_N \sim 1$ ($k_N = 0.91$ for $n = 3$ polytrope and $\gamma_{\rm ad} = 4/3$ (Kazhdan & Murzina 1992). The initial velocity u_2 is given by equation (12). In the ultrarelativistic case,

$$\Gamma_f = \Gamma_2^b . \qquad (25)$$

The power b as obtained in the analytical solutions is $b = 1 + 3^{1/2} = 2.73$ for the plane shock wave (Johnson & McKee 1971) and $b = 2.0$ for the spherical one (Eltgroth 1972). In our calculations, we shall adopt $2.0 \leq b \leq 2.73$.

One can approximate both relativistic and nonrelativistic cases by the relation

$$\Gamma_f = \Gamma_2^b + (4k_N^2 - b) \frac{\Gamma_2 - 1}{\Gamma_2^2} . \qquad (26)$$

Therefore, the gas element located in the preshock shell at a distance r, which we describe by the fraction of external mass F given by equation (10), is accelerated first to the Lorentz factor $\Gamma_2(F)$, given by equations (11) and (17), and then to the Lorentz factor Γ_f, given by equation (26).

The number of nucleons accelerated to a kinetic energy per nucleon higher than $E_K = (\Gamma_f - 1) m_{\rm H} c^2$ is given by

$$Q_N(>E_K) = \frac{[F(E_K) - F_{\rm min}] M_s}{m_{\rm H}} . \qquad (27)$$

Therefore, $Q_N(>E_K)$ gives us the integral spectrum of hydrodynamically accelerated nuclei.

For the nonrelativistic case $\Gamma_f - 1 \ll 1$, we have

$$F(E_K) = F_i (E_K/E_i)^{-\gamma_{\rm nr}^{\rm int}} , \qquad (28)$$

where $\gamma_{\rm nr}^{\rm int} = 2/(3a)$ and, numerically, $\gamma_{\rm nr}^{\rm int} = 3.3(2.9)$ for $a = 0.2(0.232)$. The energy parameter E_i is given by

$$E_i = \tfrac{72}{49} (\Gamma\beta)_i^2 m_{\rm H} c^2 = 3.4 \text{ MeV nucleon}^{-1} . \qquad (29)$$

For ultrarelativistic case $\Gamma_f \gg 1$, one obtains

$$F(E) = K \left(\frac{E}{m_{\rm H} c^2} \right)^{-\gamma_{\rm rl}^{\rm int}} , \qquad (30)$$

where $K = 1.1 \times 10^{-11}$ and $K = 2.3 \times 10^{-10}$ for $a = 0.2$ and $a = 0.232$, respectively. The exponent of the spectrum in the ultrarelativistic case is $\gamma_{\rm rl}^{\rm int} = 4/(3ab)$, and, numerically, it is equal to $\gamma_{\rm rl}^{\rm int} = 3.3$ for $a = 0.2$ and $b = 2.0$, and to $\gamma_{\rm rl}^{\rm int} = 2.1$ for $a = 0.232$ and $b = 2.73$. Note that in all cases, the values of γ are given for integral spectra. The parameters of the spectra of hydrodynamically accelerated particles are given in Table 3.

Table 3 shows that in the compact white dwarf case, the Lorentz factor of hydrodynamically accelerated nuclei reaches the values of $\Gamma_f \sim$ 100–1000, while for the extended white dwarf, the maximum values of Lorentz factors are less, $\Gamma_f \sim$ (10–100). The fraction 10^{-9}–10^{-10} of the total mass of the star is accelerated to the Lorentz factors $\Gamma_f \geq 2$. The net energy of these particles reaches 10^{44}–10^{45} ergs. The net energy of the subrelativistic particles with $E_K >$ 500 MeV nucleon^{-1} is 10^{45}–10^{46} ergs. The total number of nucleons Q_N accelerated to energies higher than E_K is given in Table 3. The particles with these energies can generate gamma radiation through production of neutral pions. E_γ^m in Table 3 refers to the end of the power-law spectrum.

During the expansion of the relativistic shell, its optical depth τ decreases. When $\tau \gg 1$, the energy losses of the shell, caused by radiation, are small. The thermal energy of the shell and the work of the pressure of the internal layers are converted into kinetic energy of the shell, and these pro-

TABLE 3

VALUES OF THE PARAMETERS OF HYDRODYNAMICALLY ACCELERATED MATTER AT THE END OF THE ACCELERATION PHASE

	COMPACT WHITE DWARF				EXTENDED WHITE DWARF			
	$a = 0.2$		$a = 0.232$		$a = 0.2$		$a = 0.232$	
PARAMETERS	$b = 2.0$	$b = 2.73$	$b = 2.0$	$b = 2.73$	$b = 2.0$	$b = 2.73$	$b = 2.0$	$b = 2.73$
Γ_f	45	170	230	1500	12	27	44	160
$E_K^{\max}$ (GeV)	42	158	214	1400	11	25	41	150
$\gamma_{\rm rl}^{\rm int}$	3.3	2.4	2.9	2.1	3.3	2.4	2.9	2.1
$Q_N(E_K > 500$ MeV)	3.9(48)	3.9(48)	4.0(49)	4.0(49)	2.8(48)	2.8(48)	2.9(49)	2.9(49)
$Q_N(E_K > 940$ MeV)	5.2(47)	5.2(47)	7.0(48)	7.0(48)	3.7(47)	3.7(47)	5.0(48)	5.0(48)
$Q_N(E_K > 9.4$ GeV)	1.4(43)	1.8(44)	8.6(44)	7.5(45)	1.0(43)	1.3(44)	6.1(44)	5.4(45)

NOTE.—The notation $a(b)$ signifies $a \times 10^b$.

cesses are taken into account in the calculations mentioned above. Because of the work of the inner layers, the total energy of the outer layer in the end of the adiabatic expansion is larger than its total energy at the moment when the shock crossed it.

When the optical depth of the shell decreases to $\tau \leq 1$, the remaining thermal energy will be mostly radiated away, and at some conditions a second precursor gamma-ray burst might be produced. The physics of this second burst is similar to that of the prompt precursor of gamma burst in the fireball models (Goodman 1986; Paczyński 1986; Shemi & Piran 1990; Meszaros & Rees 1993).

5. GAMMA-RAY BURST

The expansion of the relativistic shell after the adiabatic phase resembles the propagation of a powerful beam of relativistic particles. They have energies up to 1000 GeV nucleon^{-1} and total energy 10^{45}–10^{46} ergs. These particles interact with the accreting gas, producing the pions and gamma rays from neutral pion decays. The distribution of the gas around the white dwarf is described by equation (4) for $r \geq R_{\rm sh}$ and equation (5) for $r \leq R_{\rm sh}$. The numerical parameters for this distribution are listed in Table 1.

Our calculations for production of photons (through $pp \rightarrow \pi^0 \rightarrow \gamma\gamma$) are performed for two energy regions: $E_K^{\min} \leq E_K \leq E_c$ and $E_K > E_c$, where $E_K^{\min} = 0.4$ GeV nucleon^{-1} and $E_c = 10$ GeV nucleon^{-1}.

For the low-energy region 0.4–10 GeV nucleon^{-1}, we calculate the total number of photons Q_γ of all energies produced in the burst at angle θ relative to the direction to the secondary companion:

$$\frac{dN_\gamma(\theta)}{d\Omega} = 2\int_{R_S}^{\infty} dr n_N(r, \theta) \int_{E_K^{\min}}^{E_c} dE_K \frac{Q_N(E_K)}{4\pi} \langle \xi\sigma(E_K)\rangle , \quad (31)$$

where $n_N(r, \theta)$ is the number density for the nucleons in the gas, $Q_N(E_K)$ is the total number of accelerated nucleons with energy E_K per nucleon, and $\langle \xi\sigma(E_K)\rangle$ is the cross section for π^0 production in $NN-$ collisions. For this cross section, we use the parametrization of experimental data for $p + p \rightarrow \pi^0 +$ all, given by Dermer (1986). For energies $E > 10$ GeV nucleon^{-1} we shall use the scaling approximation for the cross section:

$$\frac{d\sigma(E_N, E_\pi)}{dE_\pi} = \frac{\sigma_0}{E_\pi} f_\pi(x) , \quad (32)$$

where $x = E_\pi/E_K$, E_π is the pion energy, $\sigma_0 = 32$ mb, and

$$f_\pi(x) = 0.67(1 - x)^{3.5} + 0.5e^{-18x} . \quad (33)$$

This approximation describes very well the experimental data. The differential spectrum of produced gamma radiation is calculated as

$$\frac{dN_\gamma(E_\gamma, \theta)}{d\Omega\, dE_\gamma} = \sigma_0 \int_{R_S}^{\infty} dr n_N(r, \theta) \times \int_{E_\gamma}^{E_K^{\max}} \frac{dE_K}{E_K} \frac{Q_N(E_K)}{4\pi} \int_{E_\gamma/E_K}^{1} \frac{dx}{x^2} f_\pi(x) , \quad (34)$$

where $E_K^{\max}$ is the maximum energy for every nucleon in the spectrum of accelerated protons. The results of the calculations are displayed in Figures 2–4.

In Figure 2, the column density of gas in the binary system is plotted as a function of angle θ, relative to the line between the centers of the stars. One can see that for all angles, the main contribution comes from the region $r \leq R_{\rm sh}$ (the horizontal lines). Only at small angles is the contribution of the stellar wind appreciable; however, for $\theta > 5°$ it does not exceed 10%.

The column density in both our models is considerably less than the nuclear interaction length ($x_N \sim 40$–50 g cm^{-2}) and high-energy gamma-ray absorption length ($x_{\rm abs} \sim 70$ g cm^{-2}). Therefore, the column density dependence $x(\theta)$, shown in Figure 2, coincides exactly with the total photon flux dependence $\dot{N}_\gamma(\theta)$.

More explicitly, the distribution of the gas in the binary system is displayed in Figure 3, where the density of the gas, ρ, is plotted against the distance from the white dwarf. The position of the shock with the transition to the stellar wind density is clearly seen there.

In Figure 3, the density profile coincides with the time profile of the gamma-ray burst. The energy-integrated

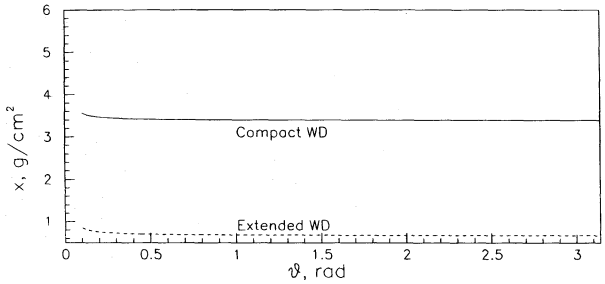

FIG. 2.—Total column density of gas in the binary system as a function of angle θ, relative to the binary axis (line between the centers of two stars).

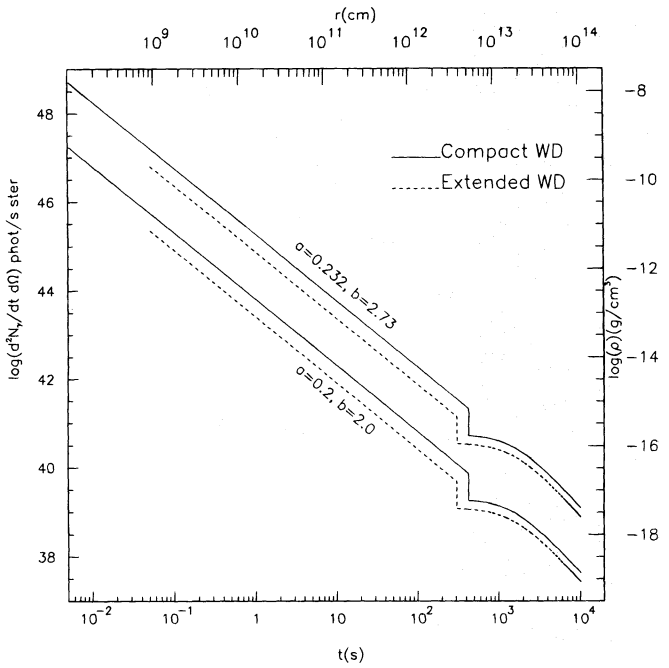

FIG. 3.—Time profile of the gamma-ray burst. On the left ordinate axis the energy-integrated number of photons emitted for every 1 s and 1 sr is displayed. Emission time t shown in the lower abscissa axis is defined as the time of flight $t = (r - R_S)/v_N$ for the nuclei, with energy per nucleon E_K at the maximum of the production rate $\langle \xi\sigma(E_K)\rangle N(E_K)$. The time profile curve (*full upper curve*) coincides with the density distribution $\rho(r)$ given by the values on the right ordinate axis and the upper abscissa axis. Minimum distance corresponds to the surface of the star. Curves are given for the cases of compact and extended white dwarfs and for $\theta = 90°$. Note that the gamma radiation is almost spherically symmetrical (see Fig. 2).

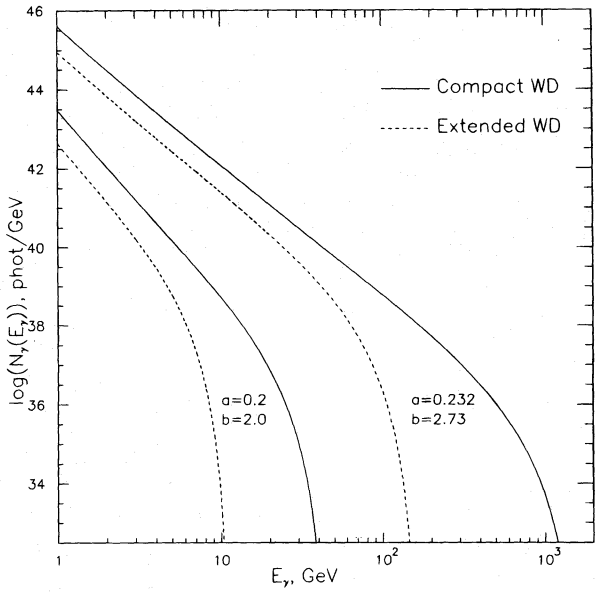

FIG. 4.—Energy spectra at $E_\gamma \geq 1$ GeV for compact white dwarf (*solid curves*) and extended white dwarf (*dashed curves*). Corresponding values of the parameters a and b are shown. Plotted quantities are the number of photons in the burst for every 1 GeV.

number of photons produced, $d\dot{N}_\gamma/d\Omega$, for given θ (the angle relative to the binary axis) is shown as a function of the production time t in the binary system. This time is equal to the time of flight, $t = (r - R_S)/v_N$, for the nuclei with energy per nucleon E_K at the maximum of the production rate $\langle \xi\sigma(E_K)\rangle N(E_K)$.

The flux decreases with time approximately as $(t + t_0)^{-3/2}$, where $t_0 = R_S/v_N$. Duration of the burst for a remote observer is different at different energies of photons. The peak in the spectrum, centered at $E_\gamma \approx 70$ MeV, is produced by pions with small kinetic energies, and therefore photons are emitted isotropically. The observed duration is determined by the difference in the time of flight for photons arriving radially ($\theta = 0$) and from the edge of the limb ($\theta \sim \bar{R}/r$), where $\bar{R} = (R_s R_{sh})^{1/2}$ is the mean length of the p-interaction region and r is the distance between the observer and the source. It gives the duration $(\Delta t)_{obs} \sim 1$ s (3 s) for the compact (extended) model. For the high-energy photons produced by the protons with $\Gamma \gg 1$, the burst is considerably shorter. The simple kinematic estimates show that the photons are, on average, emitted at an angle $\theta \approx 0.3/\Gamma$ relative to the direction of the proton propagation (i.e., the radial direction). The duration, determined again as the maximum difference of time of flight, is

$$(\Delta t)_{obs} = \frac{\bar{R}}{c}\frac{\theta^2}{2} \approx 0.05\,\frac{\bar{R}}{c}\,\Gamma^{-2}\,.$$

In particular, for photons with $E_\gamma \sim 1$ GeV, the observed duration of the burst is $(\Delta t)_{obs} = 5 \times 10^{-4}(1 \times 10^{-3})$ s for the compact (extended) model (see Fig. 4).

The spectrum of the high-energy gamma radiation is very steep: it has the same power exponent $\gamma_{rl}^{int} + 1$ as the differential spectrum of accelerated particles. At $E_\gamma \simeq 70$ MeV, it has the well-known peak from the decays of pions at rest. Therefore, the gamma-ray burst is detected most effectively at $E_\gamma \sim 100$ MeV. However, at $E_\gamma \geq 1$ GeV the signal is also detectable. The total number of emitted photons varies from $N_\gamma \sim 4.5 \times 10^{47}$ (for the compact white dwarf model) to $N_\gamma \sim 3.5 \times 10^{45}$ (for the extended white dwarf model; Table 4). The corresponding fluences are in the range 0.3–40 photons cm^{-2}, for a distance of 10 kpc.

TABLE 4

PARAMETERS OF THE MAIN GAMMA-RAY BURST

	COMPACT WHITE DWARF				EXTENDED WHITE DWARF			
	$a = 0.2$		$a = 0.232$		$a = 0.2$		$a = 0.232$	
PARAMETERS	$b = 2.0$	$b = 2.73$	$b = 2.0$	$b = 2.73$	$b = 2.0$	$b = 2.73$	$b = 2.0$	$b = 2.73$
W_γ (ergs)	2.6(42)	6.2(42)	3.2(43)	7.2(43)	5.6(41)	1.4(42)	7.0(42)	1.6(43)
N_γ^{tot} (photon)	1.5(46)	3.9(46)	2.0(47)	4.5(47)	3.5(45)	8.8(45)	4.4(46)	1.0(47)
E_γ^m (GeV)	4.2	16	21	140	1.0	2.5	4.1	15
N_γ(10 GeV) (photon GeV^{-1})	5.0(38)	2.0(40)	6.0(40)	1.0(42)	4.0(33)	4.0(37)	8.0(37)	2.0(41)

NOTE.—The notation $a(b)$ signifies $a \times 10^b$.

6. DISCUSSION AND CONCLUSIONS

We study SN Ia explosions in a binary system consisting of a compact star (white dwarf) and a late-type secondary companion (red giant). The accretion onto a white dwarf causes the ignition of nuclear reactions and the ejection of the shell. The accretion is assumed to be in the wind regime, with the Roche lobe of the secondary companion not filled. The accretion flow is terminated by the shock at distance $r = R_{sh}$ from the white dwarf. The radius of the shock R_{sh} is of the order of the accretion radius R_{acc} (see eq. [1]). At $r \leq R_{sh}$, we assume a radial accretion flow to the white dwarf.

Gas within the shock radius comprises the main fraction of the target for gamma-ray production. Its density and column density are determined mostly by the mass of the compact star M_S and by the parameters of the stellar wind, its density ρ_W, and its velocity u_W. We take the density distribution and the radius of the shock R_{sh} from the numerical calculations by Taam et al. (1991). The values of the column density of the gas as a function of θ, the angle relative to the line between the centers of the two stars, are given in Figure 2. The mean value of the column density is $x = 3.4$ g cm^{-2} for the compact white dwarf model and $x = 0.67$ g cm^{-2} for the extended white dwarf model (Table 1).

The particles in our model are accelerated hydrodynamically. We distinguish two stages of acceleration. The first is connected with the propagation of the shock through the shell. The acceleration occurs if the density in the shell decreases sharply outward: e.g., $\rho(r) \sim r^{-m}$, with $m > 3$. In this case, the shock propagates with increasing velocity, leaving the hot gas with a large radial velocity behind the shock front. Following Colgate (1984), we describe the position of the layer considered by the amount of the gas in front of it. In other words, we use the fraction $F = M(>r)/M_s$, where $M(>r)$ is the mass of the shell at the distance greater than r and M_s is the mass of the star. The Lorentz factor of the gas in the shell at a given F can be found from equations (11) and (17). The uncertainties for these calculations are mainly connected with the parameter a, which is defined by equation (9); we expect that it varies from 0.2 to 0.232 (Gnatyk 1985).

The second stage of acceleration begins when the shock reaches the outer edge of the star. The shell adiabatically expands into a low-density medium, and the pressure accelerates the shell. The thermal energy of the gas and the work of the pressure are converted into kinetic energy of the shell. This stage terminates when the shell becomes transparent and the thermal energy is radiated away. The Lorentz factor of the shell acquired at this stage is $\Gamma_f = \Gamma_2^b$, where Γ_2 is the Lorentz factor at the end of the first stage and b is a parameter which varies from $b = 2.0$ for the spherical wave (Eltgroth 1972) to $b = 2.73$ for the plane wave (Johnson & McKee 1971). The value of b gives the largest uncertainties for the calculations of this stage of acceleration.

The numerical predictions are given for two models: compact white dwarf ($M_S = 1\ M_\odot$ and $R_S = 1 \times 10^8$ cm) and extended white dwarf ($M_S = 1\ M_\odot$ and $R_S = 1 \times 10^9$ cm; Table 1). The former is more favorable for particle acceleration. For given values of the parameters a and b, the spectrum of the accelerated nuclei has a power-law form with the integral exponent $\gamma_{rl}^{int} = 4/(3ab)$. In the compact white dwarf model, with $a = 0.232$ and $b = 2.73$, we obtain $\gamma_{rl}^{int} = 2.1$, the maximum energy of particles $E^{max} \sim 1400$ GeV nucleon^{-1}, and the total energy of particles with $E_K > 500$ MeV nucleon^{-1}, $W \sim 3 \times 10^{46}$ ergs.

For the other extreme case of the extended white dwarf model and the values $a = 0.2$, $b = 2.0$, the acceleration has a minimal efficiency: $\gamma_{rl}^{int} = 3.3$, $E^{max} \sim 11$ GeV nucleon^{-1}, and the total energy is $W \sim 2 \times 10^{45}$ ergs.

Two precursor gamma-ray bursts are expected. The first is connected with the shock breakout when the shock traverses the outer thin layer transparent for radiation. The thermal radiation accumulated in the shock front is radiated away when the shock reaches the surface of the star. The thermal photons are blueshifted because of the relativistic expansion of the shell, and their typical energies reach $E \sim \Gamma_2 kT_2 \sim 300(1000)$ keV for the $a = 0.2(0.232)$ compact model and $E \sim 47(120)$ keV for the extended one. Relativistic effects probably convert the Planck spectrum in the power-law spectrum (Shemi 1994). The total energy of the burst in the reference frame of the observer is $W_{burst} \sim 2 \times 10^{38}(2 \times 10^{37})$ ergs for the $a = 0.2(0.232)$ compact model and $W_{burst} \sim 6 \times 10^{40}(3 \times 10^{41})$ ergs for the extended one. The duration of the burst for a distant observer is given by equation (24). This time is typically very short, $\Delta t \sim 10^{-5}$ s, for a compact white dwarf.

The second precursor burst might appear at the last stage of the adiabatic expansion of the shell of accelerated particles behind the shock, when this shell becomes transparent and its thermal energy is radiated away.

The main gamma-ray burst is produced by the interaction of the accelerated nuclei with the accreting gas. The major part of the calculated flux corresponds to the interaction of the nuclei with the gas within the shock radius R_{sh}. Protons are produced as a result of the neutral pion decay. At high energies, the gamma-ray spectrum is very steep: it is characterized by the same spectrum exponent of the accelerated particles (see eqs. [28] and [30]). At low energy, the spectrum has the usual peak at $E_\gamma \simeq 70$ MeV. Most of the photons have energies $E_\gamma \geq 70$–100 MeV. The maximum energies of photons are of order $E_\gamma \sim 4$–140 GeV, depending on the values of the parameters a and b for the compact white dwarf model, and $E_\gamma \sim 1$–15 GeV for the extended white dwarf model. The total number of photons in the burst is $N_\gamma^{tot} \sim 2 \times 10^{46}$–$5 \times 10^{47}$ for the compact white dwarf and $N_\gamma^{tot} \sim 4 \times 10^{45}$–$1 \times 10^{47}$ for the extended white dwarf.

We want to emphasize here that in our calculations we chose the parameters very conservatively, deliberately trying not to overestimate the predictions. The accelerated particles traverse only about 3.5 g cm^{-2} and 0.67 g cm^{-2} of the matter in compact and extended models, respectively. For acceleration, we used very conservative assumptions too, which resulted in a steep spectrum and low-maximum energies of the accelerated particles in comparison with the Colgate (1984) calculations.

The predicted burst radiation can be easily detected if SN Ia occurs in our Galaxy. For a distance 10 kpc from Earth, the typical flux of gamma radiation at $E_\gamma \geq 100$ MeV is 1 photon cm^{-2} and for $E_\gamma \geq 10$ GeV it is 10^{-4}–10^{-3}photon cm^{-2}.

The duration of the burst is different in different energy intervals. At $E_\gamma \geq 100$ MeV, it is of the order of 1s. For the high-energy photons at $E_\gamma \geq 10$ GeV, it reduces to 10^{-5} s. Thus, we predict a novel type of gamma-ray bursts with properties quite different from those currently observed.

Since these bursts are a rare phenomenon, their detection needs the patrol service.

The hydrodynamical mechanism for gamma-ray bursts, which we put forward here for SN I, can work for other objects as well. The crucial condition for the hydrodynamical mechanism is a large density gradient, which provides acceleration of the shock front. The accelerated particles produce a detectable gamma-ray burst even in the case of a relatively small column density of the target. As an example, we mention the accretion-induced collapse of a white dwarf to a neutron star (see Woosley & Baron 1992, and references therein). According to their calculations, 7×10^{-6} part of the whole dwarf mass acquires a velocity higher than $u_f = 38{,}000$ km s^{-1}. Then the maximum velocity of the shock is given by $(\Gamma_{sh}\beta_{sh})_{max} = 2.8(5.2)$ for $a = 0.2(0.232)$, which is only a factor 1.5 smaller than in the case of our extended model. Therefore, we expect here the gamma-ray burst too. Another example is probably give by the explosion of a neutron star below the minimum mass (Blinnikov et al. 1990; Colpi, Shapiro, & Teukolsky 1993). These examples illustrate the attractiveness of the hydrodynamical mechanism for astrophysical applications.

B. Hnatyk is grateful to Laboratori Nazionali del Gran Sasso and, in particular, to the director, P. Monacelli, for their hospitality.

REFERENCES

Berezinsky, V. S., & Prilutsky, O. F. 1985, Proc. 19th Int. Cosmic-Ray Conf., Vol. 1-OG, 29
Blandford, R. D., & McKee, C. F. 1976, Phys. Fluids, 19, 1130
Blinnikov, S. I., Imshennik, V. S., Nadyozhin, D. K., Novikov, I. D., Perevodchikova, T. V., & Polnarev, A. G. 1990, Soviet Astron., 34(6), 595
Blinnikov, S. I., & Nadyozhin, D. K. 1991, in Supernovae, ed. S. E. Woosley (New York: Springer), 213
Colgate, S. A. 1974, ApJ, 187, 333
———. 1984, Adv. Space Res., 4, 367
Colgate, S. A., & Johnson, N. H. 1960, Phys. Rev. Lett., 5, 235
Colpi, M., Shapiro, S. L., & Teukolsky, S. A. 1993, ApJ, 414, 717
Dermer, C. D. 1986, A&A, 157, 223
Eltgroth, P. G. 1972, Phys. Fluids, 15, 2140
Ensman, L., & Burrows, A. 1992, ApJ, 393, 742
Fryxell, B. A., & Taam, R. E. 1988, ApJ, 206, 847
Fujimoto, M. Y., & Taam, R. E. 1982, ApJ, 260, 249
Gnatyk, B. I. 1985, Soviet Astron. Lett., 11, 331
Goodman, J. 1986, ApJ, 308, L47
Grassberg, E. K., Imshennik, V. S., & Nadyozhin, D. K. 1971, Ap&SS, 10, 28
Hoyle, F., & Lyttleton, R. A. 1939, Proc. Cambridge Phil. Soc., 35, 405
Imshennik, V. S., & Nadyozhin, D. K. 1988, Soviet Astron. Lett., 14(6), 449
Imshennik, V. S., & Nadyozhin, D. K. 1989, Astrophys. Space Phys. Res., 8, 1
Johnson, M. H., & McKee, C. F. 1971, Phys. Rev. D, 3, 858
Kazhdan, Ya. M., & Murzina, M. 1992, ApJ, 400, 192
Kenyon, S. J., Livio, M., Mikolajewska, J., & Tout, C. A. 1993, ApJ, 407, L81
Khokhlov, A., Müller, E., & Höflich, P. 1993, A&A, 270, 223
Matsuda, T., Inoue, M., & Sawada, K. 1987, MNRAS, 226, 785
Meszaros, P., & Rees, M. J. 1993, ApJ, 405, 278
Munari, U., & Renzini, A. 1992, ApJ, 397, L87
Nomoto, K. 1982, ApJ, 253, 798
Paczyński, B. 1986, ApJ, 308, L43
Rees, M. J. 1966, Nature, 211, 468
Shemi, A. 1994, MNRAS, 269, 1112
Shemi, A., & Piran, T. 1990, ApJ, 365, L55
Taam, R. E., & Fryxell, B. A. 1988, ApJ, 327, L73
———. 1989, ApJ, 338, 297
Taam, R. E., Fu, A., & Fryxell, B. A. 1991, ApJ, 371, 696
Weaver, T. A. 1976, ApJS, 32, 233
Wheeler, J. C., & Harkness, R. P. 1990, Rep. Prog. Phys., 53, 1467
Woosley, S. E., & Baron, E. 1992, ApJ, 391, 228
Woosley, S. E., Taam, R. E., & Weaver, T. A. 1986, ApJ, 301, 601